Catalysis Today xxx (xxxx) xxx

Contents lists available at ScienceDirect

Catalysis Today

journal homepage: www.elsevier.com/locate/cattod

Electrospinning synthesis and characterization of nanofibers of Co, Ce and mixed Co-Ce oxides. Their application to oxidation reactions of diesel soot and CO

M. Ángeles Stegmayer [a], Silvia Irusta [b], Eduardo E. Miró [a], Viviana G. Milt [a,*]

[a] Instituto de Investigaciones en Catálisis y Petroquímica, INCAPE, Universidad Nacional del Litoral, CONICET, Facultad de Ingeniería Química, Santiago del Estero, 2829 - 3000, Santa Fe, Argentina
[b] Department of Chemical Engineering, Instituto de Nanociencia y Materiales de Aragón (INMA), CSIC-Universidad de Zaragoza, Zaragoza, 50009, Spain

ARTICLE INFO

Keywords:
Ceria and cobalt nanofibers
Electrospinning
Cobalt spinel
Soot oxidation
CO oxidation

ABSTRACT

Co, Ce and Co-Ce nanofibers were synthesized by the electrospinning method. To obtain mixed fibers, Co was incorporated in two ways: one step synthesis and sequential synthesis. Nanofibers were applied to two reactions: gas-solid (CO oxidation) and solid-solid-gas (combustion of diesel soot). Different activity trends were observed in both reactions. For soot combustion, Co-Ce nanofibers were more active either than Co or Ce nanofibers. For CO oxidation instead, the activity order was Co > Co-Ce > Ce. Moreover, in the case of soot combustion, for all samples the temperature of maximum combustion rate occurred at a relatively narrow range (350−390 °C). On the contrary, for CO oxidation the temperature range for T_{50} was notably wider (150−325 °C). The high activity shown for all the samples for soot oxidation is related to the multiple contact points between the fibers and the soot particles, and the trend observed for CO oxidation related to the higher redox capacity of Co, as observed from CO-TPR experiments.

1. Introduction

Nowadays, new concepts about the design of catalytic support structures and structured reactors are emerging with the aim of optimize the production in chemical industries or the contaminants abatement efficiency in environmental applications. Many of the new structures are based on fibers made from different materials, which have several beneficial aspects in reaction engineering applications. Among them, fibrous substrates can be fitted to various geometries due to their flexibility and can be made of different materials as ceramic, metal and glass [1,2].

Ceramic fibers of nanometric size have advantages such as large porosity, lower pressure drop, empty space generation, high aspect ratio, high surface/volume ratio and lower cost compared to microreactors [3]. Among the different methods used to produce nanometric fibers, electrospinning is a simple and powerful technique involving the use of different materials. Ceramic fibers can be obtained after calcination of the composite material obtained by electrospinning a mixture made of a polymer and an inorganic precursor [4]. Recently, Dai et al. [5] reported that shape and diameter manipulation in porous CeO_2 nanofibers can be successfully achieved, with high quality and high reproducibility, by simply tuning the electric field strength during electrospinning.

These nanofibers have been used in various catalytic processes, for example photocatalysis, oxidation of toluene and propane, oxidative coupling of methane [6]. Another important application of nanofibers has been the reduction of pollutants present in diesel vehicle emissions containing nitrogen oxides, carbon monoxide, unburned hydrocarbons and soot particles [3,7]. Commercial catalysts used in the cleaning of these vehicle exhaust emissions mainly use noble metals (Pt, Au, Pd), which are expensive and susceptible to sintering and poisoning. Thus, the use of transition metals is increasingly considered, being ceria based catalysts among the most studied materials for replace the noble ones for the oxidation of CO, VOCs and carbonaceous particles [8,9]. This is mainly due to the high oxygen storage capacity (OSC) and oxygen mobility of ceria [10]. A great deal of formulations includes modification of CeO_2 with other species; both alkali metals and rare earths were studied to modify ceria [11,12].

CO oxidation and soot combustion are among the most studied catalytic reactions of environmental interest due to the high toxicity of both

* Corresponding author.
E-mail address: vmilt@fiq.unl.edu.ar (V.G. Milt).

https://doi.org/10.1016/j.cattod.2020.12.018
Received 23 September 2020; Received in revised form 30 November 2020; Accepted 21 December 2020
Available online 28 December 2020
0920-5861/© 2020 Elsevier B.V. All rights reserved.

contaminants [13]. However, despite both being deep oxidation reactions, they have different characteristics. While CO oxidation is a classical heterogeneous gas-solid catalytic reaction, soot oxidation involves multiple contact points between two solid phases and the gaseous one. Thus, the increase of the soot-to-catalyst contact plays a key role in determining the catalytic efficiency.

With respect to soot oxidation, Liu et al. [14] propose that mainly five different kinds of ceria-based catalysts with special morphologies can be applied: three dimensionally ordered macroporous (3DOM) catalysts, fiber catalysts, nanometric catalysts, core-shell catalysts and exposed lattice plane-controlled catalysts, being the former three those that increase the contact area between catalysts and soot particles, thus exhibiting better catalytic activities than the conventional catalysts. In this vein, the combination of the advantages of fiber catalysts with the oxidizing properties of cerium oxide constitutes an interesting approach for the development of efficient catalytic systems devoted to the abatement of diesel contaminants. Moreover, it has been reported that the addition of a transition metal oxide like CuO or Co_3O_4 promotes the oxidizing activity [7,9,15].

Catalytic materials based on Co and Ce oxides mixtures have been proven to be efficient for deep oxidation reactions [2,3,16]. Taking this fact into account, and the advantages of fiber structures, the present work aimed to develop efficient catalytic nanofibers made of Co oxide, Ce oxide and the mixed Co-Ce fibers using the electrospinning technique for their application in the catalytic oxidation of environmental pollutants. We have selected the oxidation of carbon monoxide and the combustion of diesel soot, both components present in the gases emitted by cars. As said above, the selected reactions occur through different mechanisms, and an important objective of this work is to insight in the role of fibers as catalysts for solid-solid and gas-solid catalytic oxidation reactions. To this end, the catalytic behavior was studied by means of Temperature-Programmed Oxidation for soot and CO oxidation. Catalytic fibers were characterized using a series of techniques: SEM, EDX, XPS, XRD, LRS, BET, ATR-FTIR and CO-TPR.

2. Experimental

2.1. Catalysts preparation

2.1.1. Preparation of nanofibers by the electrospinning method

Cobalt, ceria and cobalt-ceria nanofibers were made using the electrospinning method. In the case of Co-Ce mixed fibers, cobalt was incorporated during the synthesis itself, or by wet impregnation over ceria electrospun fibers.

CeO_2 fibers were prepared in a 2.2.D-500 YFlow electrospinner, using $Ce(NO_3)_3$ as precursor and polyvinylpyrrolidone (PVP, M_w = 1.300.000) to generate a fibrous structure. 0.29 g $Ce(NO_3)_3.6H_2O$ (Sigma Aldrich) were dissolved in an ethanol (10 mL)–water (2 mL) mixture under magnetic stirring for 15 min. Then, 1 g PVP was added and the solution was kept under magnetic stirring overnight. The viscous Ce-PVP solution was loaded into a syringe connected with the inner part of the coaxial needle, and ethanol was used as shell liquid to avoid needle clogging. The tip was placed at 25 cm from the collector plate. Pumps were set at 1 mL/h for the inner solution and at 0.2 mL/h for the outer liquid. A voltage of -2.1 kV was connected to the collector plate and a positive voltage of 9.5 kV was connected to the metallic needle [4]. As-spun fibers were calcined at 600 °C for 5 h with a heating rate of 0.5 °C/min in order to guarantee the complete removal of polymers. This catalyst was called Ce. Using the same technique described above, cobalt fibers were synthesized using $Co(NO_3)_2.6H_2O$ (Sigma Aldrich) as precursor, applying a potential difference of 14 kV. These prepared fibers were denoted as Co.

Similarly, Co-Ce mixed fibers were synthesized mixing Ce $(NO_3)_3.6H_2O$ and $Co(NO_3)_2.6H_2O$ in two proportions: 2 or 12 wt.% Co (referred to CeO_2). The potential difference applied for Co-Ce fibers was approximately 11 kV. These samples were called: Co(2 %)Ce* and Co(12 %)Ce*, where the asterisk indicates that cobalt was added during the synthesis step (one step synthesis).

2.1.2. Deposition of cobalt on ceria fibers

Besides studying the addition of cobalt during the fiber synthesis, the incorporation of cobalt through the wet impregnation method was studied, using the electrospun ceria fibers as support (sequential synthesis). For this, Ce fibers were added to a $Co(NO_3)_2$ solution under continuous stirring while heating at 90 °C until dryness. The resulting solid was dried at 120 °C for 24 h and then calcined in air at 600 °C for 2 h heating at 1 °C/min. Varying the concentration of cobalt in the solution, catalysts with 2 and 12 wt.% Co were prepared on the ceria supports, which were named as Co(2 %)Ce and Co(12 %)Ce, respectively.

2.2. Catalysts characterization

The fibers were carefully characterized by XRD, LRS, SEM, EDX, ATR-FTIR, BET, CO-TPR and XPS.

The diffractograms were obtained with a Shimadzu XD-D1 equipment with monochromator, using Cu Kα radiation at 2°/min, detection limit 1 wt.%. CeO_2 and Co_3O_4 crystallite sizes were calculated using the main peak of the diffractograms and the Scherrer equation.

Laser Raman spectra were obtained in a Horiba JOBIN YVON LabRAM HR equipment. The excitation source was the 514.5 nm line of a Spectra 9000 Photometrics Ar ion laser with the laser power set at 30 mW.

Infrared spectra were obtained using a Bruker Vertex 70 equipment, equipped with an Attenuated Total Reflectance Golden Gate. All spectra involved the accumulation of 40 scans at 4 cm^{-1} resolution.

The fibers were studied with the SEM F50 Inspect equipment and with the energy dispersive X-ray spectroscopy (EDX) equipment. In this way the size, morphology and composition of the fibers were characterized.

Temperature-programmed reduction experiments with CO as reducing agent (CO-TPR) were performed to infer on the oxygen storage capacity (OSC) and reducibility of the fibers. To this aim, 50 mg fibers were placed in a tubular quartz reactor (0.6 cm diameter) and a mixture of CO (1 %) in He (total flow, 30 mL/min) was fed, heating at 5 °C/min from room temperature to 600 °C. The gaseous product CO_2 was analyzed using a Shimadzu GC-2014 gas chromatograph. CO-TPR was performed sequentially after catalytic evaluation in CO oxidation, that is, the fibers that were previously evaluated were used (see 2.3.2). To this aim, after CO oxidation run the temperature was slow down to room temperature under He flow and then, the reducing mixture was fed and the reactor was heated, as previously described.

Surface atomic ratios and oxidation states were determined by XPS. The X-ray photoelectron analysis (XPS) was performed with an Axis Supra equipment (Kratos Tech.). The spectra were obtained by a monochromatized AlKα source (1486.6 eV) run at 15 kV and 10 mA. The samples were pretreated under vacuum at 150 °C. The effect of the electric charge was corrected considering the C1s peak (284.6 eV) as reference. The data treatment was performed with the CasaXPS program (Casa Software Ltd., UK).

The surface texture of samples was measured by nitrogen adsorption at 77 K in a Micromeritics TriStar analyzer (Micromeritics, Norcross GA). Surface area was determined using the BET equation.

2.3. Catalytic evaluation

Fibrous catalysts were studied for soot and CO oxidation reactions.

2.3.1. Soot oxidation

Soot particles, obtained from burning commercial diesel fuel (Repsol–YPF, Argentina) in a glass vessel, were dried in a stove at 120 °C for 24 h and then dispersed in n-hexane using ultrasonic bath in order to produce a homogeneous suspension. Each catalyst sample was

introduced into the soot slurry in n-hexane so that the soot-catalyst ratio was 1/20 (wt./wt.), and then placed on a heating plate until dryness. The contact thus obtained simulates the situation generated in a real diesel particulate filter (DPF) [17].

The soot combustion reaction was studied by temperature programmed oxidation (TPO) in a conventional continuous flow quartz reactor operating at atmospheric pressure. For this purpose, the soot-impregnated samples (50 mg) were loaded into a quartz reactor (i.d.: 6 mm) and heated at 5 °C/min from room temperature up to 600 °C in O_2 (18 %) + NO (0.1 %) diluted in He (total flow 20 mL/min). The exhaust gases were analyzed with a Shimadzu GC-2014 chromatograph (with TCD detector) using a Porapak Q column.

Soot conversion was calculated through the area of the CO_2 peak in the chromatogram obtained at each temperature, being negligible the amounts of CO produced. TPO curves showed produced CO_2 at each temperature and the maximum soot combustion rate was determined by the maximum in the TPO peak (T_M).

2.3.2. CO oxidation

The same flow equipment as previously described was used to study the catalytic oxidation of CO. To this aim, 50 mg nanofibers were loaded into the reactor and the conversion curves were obtained by heating the catalyst under the reactive mixture (1 % CO, 2 % O_2, diluted in He, flow rate of 30 mL/min) at 5 °C/min, from room temperature to 500 °C. CO conversion was calculated dividing the CO_2 concentration at the outlet of the reactor by the CO concentration at the inlet of the reactor. From conversion vs. temperature profiles, T_{50} values were determined, which corresponded to the temperature at which 50 % CO was converted. Additionally, apparent activation energies were calculated assuming differential conditions (CO conversions below 20 %) and pseudo-first order kinetics.

3. Results and discussion

3.1. Characterization of the catalysts

The crystalline structures of the pure supports and the supported cobalt catalysts were confirmed by XRD. In Fig. 1a, the 2θ diffraction peaks at 28.6°, 33.2°, 47.6°, 56.4°, 59.2°, 69.6°, 76.9° and 79.3°, which can be found in the XRD patterns of pure Ce and Co-Ce fibers, correspond to the cubic phase of CeO_2 with typical fluorite structure (JCPDS 34-0394). The diffractograms of Co(12 %)Ce and Co(12 %)Ce* catalysts also show peaks at 2θ = 31.3° and 36.9°, which are consistent with the main characteristic peaks of the cobalt cubic spinel phase, Co_3O_4 (JCPDS

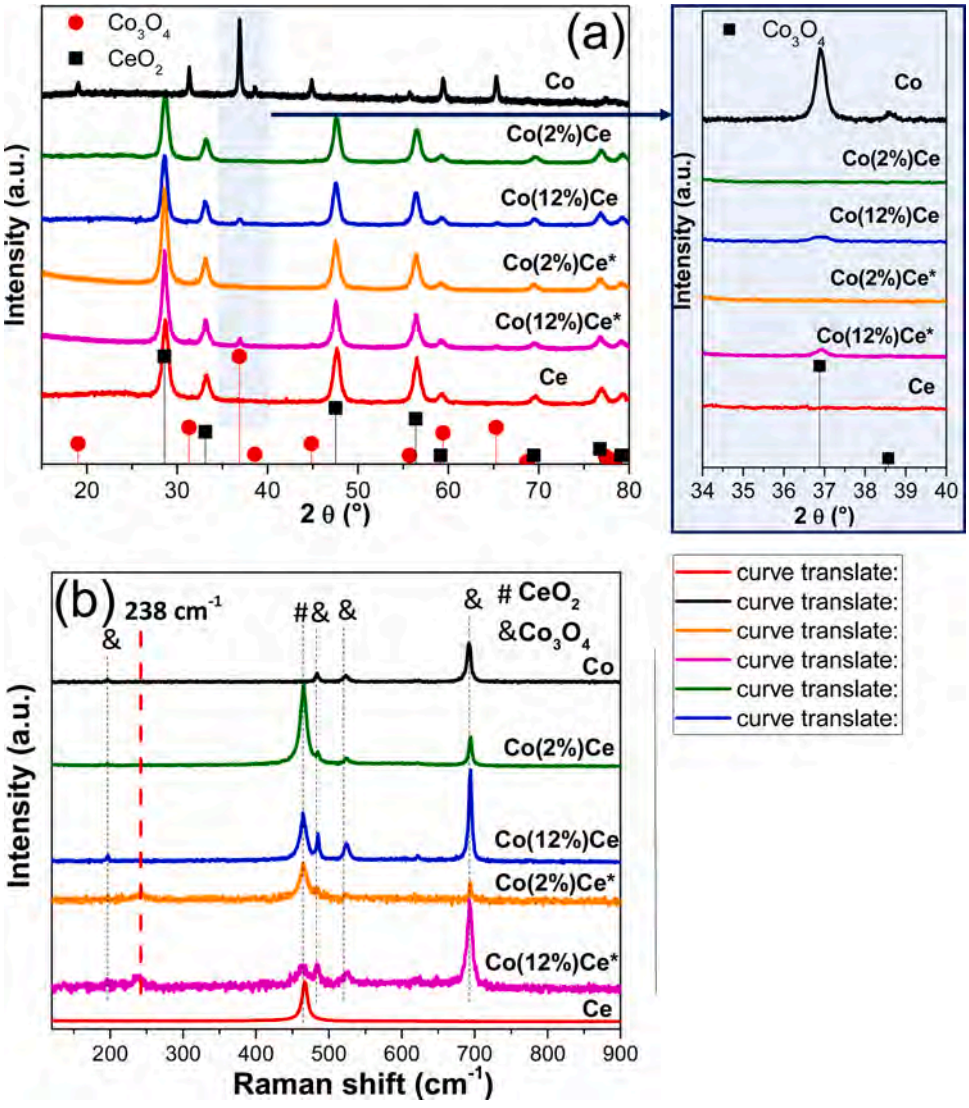

Fig. 1. XRD patterns (a) and Laser Raman spectra (b) of synthesized fibers: ceria (Ce), cobalt (Co) and CeO_2 with cobalt (Co(2 %)Ce and Co(12 %)Ce). The asterisk indicates cobalt incorporated during the fiber synthesis (one step synthesis).

42-1467). However, Co_3O_4 characteristic peaks could not be identified in catalysts with 2 wt.% Co (Fig. 1a, inset). Lin et al. reported similar results in ceria fibers with 10 wt.%Co incorporated by wet impregnation [18]. Since these percentages are higher than the detection limit of the technique, the absence of XRD signals for Co_3O_4 would imply either high Co dispersion (cobalt crystallites < 4 nm) or an amorphous phase. Besides, the introduction of some amounts of cobalt into the crystal lattice of ceria could also explain the absence of the Co phase detectable by XRD [7]. In the case of bare Co fibers, all signals observed correspond to Co_3O_4 spinel structure (2θ (°) = 19.0, 31.3, 36.9, 38.6, 44.8, 55.7, 59.4, 65.3, 68.7, 77.4 and 78.5).

Crystallite sizes were calculated from the main signals of XRD patterns (Table 1), both for CeO_2 and for Co_3O_4. CeO_2 crystallites range from 9 to 11 nm whereas cobalt crystallites were 27.5 nm for Co fibers and in the case of mixed fibers could only be determined in those samples containing 12 wt.% Co. The value calculated for Co(12 %)Ce* was very similar to that of pure cobalt fibers, and that of the impregnated sample resulted smaller (although some errors in the determination could be taking into account arising from the small peak observed for Co (12 %)Ce).

The Raman technique provides extra information on rotational and vibrational transitions of catalyst molecules. As shown in Fig. 1b, the ceria fibers show the characteristic vibrational band F_{2g} of CeO_2 at 467 cm^{-1} assigned to Ce^{4+} (triply degenerate F_{2g} vibration mode of octahedral local symmetry around CeO_2 lattice) [19]. When the cobalt content increases, ceria vibration signals weaken, and several characteristic peaks belonging to the Co_3O_4 spinel structure [20] begin to appear: 195, 482, 523, 622 and 694 cm^{-1}, being these last signals the only observed for pure Co fibers. This is in agreement with results reported by Xiang Li et al. [21], who found that when CoO_x is gradually doped in CeO_2 with the increase of Co/Ce ratio, the F_{2g} vibration signal weaken. In our case, this effect is more pronounced in the one step prepared samples due to the better and homogeneous contact between cobalt and ceria crystals. In addition, in the samples in which cobalt was incorporated during the synthesis (Co(2 %)Ce* and Co(12 %)Ce*) a small signal at 238 cm^{-1} appears. This band can be related to a cobalt-cerium compound involving Co^{2+} species [22]. This fact, is also indicative of the intimate Co-Ce interaction in the one step prepared fibers. As a matter of fact, this signal is not present in Raman spectra of impregnated samples.

The specific surface area values (S_{BET}) of all samples determined by N_2 adsorption-desorption are given in Table 1. It can be seen that the BET specific surface areas of the simple oxide fibers of Ce and Co are 94 and 23 m^2/g, respectively, which may indicate the smaller particle size of CeO_2 crystallites (9 nm and 28 nm, respectively). By incorporating cobalt by wet impregnation, the surface areas of the Co-Ce catalyst samples decrease with respect to that of the bare ceria fibers and the surface area is smaller as more cobalt is incorporated (Table 1). This is probably related to Co_3O_4 segregation in support ceria, as observed by XRD (Fig. 1). Besides, CeO_2 crystallite size increases as more amounts of cobalt are added. In contrast, Co-Ce fibers made by one step synthesis showed an increase in surface area by incorporating a higher percentage of cobalt, which implies smaller particle size as higher amounts of cobalt are incorporated. The tendency in the CeO_2 crystallite sizes is the same, independently of the method of incorporation of cobalt: the less the cobalt content, the lower the CeO_2 crystallite size. It should be noted that the Co_3O_4 crystallite size in the sample Co(12 %)Ce* is 25 nm, being very close to the values of the bare cobalt fibers (28 nm), while the Co_3O_4 crystallite size decreases to 17 nm when cobalt is incorporated by impregnation.

Fig. 2 shows SEM images of the calcined fibers. Cerium fibers have a diameter of approximately 200 nm, and they are also found to be hollow as indicated by the yellow circle in Fig. 2a. In contrast, cobalt fibers show a diameter of around 100 nm and are not hollow, which could explain the higher specific surface area developed in bare ceria fibers. In fact, the spun nanofibers containing the cobalt precursor and the PVP polymeric matrix led to Co_3O_4 nanocrystallites that after PVP removal by high-temperature calcination formed fibers resembling nanotubes (Fig. 2b). All the fibers made in this work have nanometer-sized diameters and have lengths of several microns, which are intrinsic characteristics of the ceramic fibers synthesized by the electrospinning method.

Fig. 2c shows fibers with 2 % cobalt incorporated by wet impregnation (Co(2 %)Ce). It is observed that CeO_2 fibers maintain their morphology, appearing agglomerates on these fibers. Besides, the amount of cobalt agglomerates increases as the cobalt loading is higher (Fig. 2d). The composition of these agglomerates was studied by STEM-EDX in a previous work [7], where the formation of Co_3O_4 agglomerates was found, which is also consistent with LRS results.

However, in the case of one step mixed fibers, as expected, cobalt is incorporated into the fibrous structure. Co(2 %)Ce* fibers have a diameter of between 120 and 160 nm whereas Co(12 %)Ce* fibers have a diameter of between 150 and 200 nm. The differences in the diameter of the fibers made by synthesis in one step is related to the applied voltage during the synthesis. Higher voltage was necessary for the fibers with higher cobalt content which impacted on the diameter of the fibers. The decrease in the diameter with an increase in the applied voltage could be attributed to the decrease in the size of the Taylor cone and increase in the jet velocity for the same flow rate [23].

The Co/Ce atomic ratios of all the fibers were estimated by EDX (Table 1). In the case of Co(2 %)Ce, the average value of Co/Ce calculated by EDX was 0.0365 ± 0.025 while 0.058 is the nominal atomic ratio. This observation indicates a heterogeneous distribution of cobalt in the sample that cobalt was added by wet impregnation on the ceria support fibers. For the sample containing 12 wt.% Co, even when the average value Co/Ce ratio obtained from EDX (0.304 ± 0.080) is closer to the theoretical one (0.35), the cobalt distribution is heterogeneous. On the other hand, through one step synthesis, similar atomic Co/Ce ratios were obtained by examining different regions of the samples, either with 2 or 12 wt.% Co, which agrees with a more homogeneous distribution of cobalt. The Co/Ce atomic ratios determined from EDX were 0.0573 ± 0.013 and 0.299 ± 0.001, and fit quite well with theoretical values.

The attenuated total reflectance-Fourier transform infrared spectroscopy (ATR-FTIR) was used to examine the chemical species present on the surface of fibrous catalysts at room temperature. Fig. 3 a shows

Table 1
Surface and bulk features of electrospun fibers.

Catalysts	S_{BET} (m^2/g)	CeO_2 crystallite size[a] (nm)	Co_3O_4 crystallite size[a] (nm)	Co/Ce bulk atomic ratio (EDX)	Co/Ce surface atomic ratio (XPS)	Ce^{+3}/Ce surface atomic ratio (XPS)
Ce	94	9	–	–	–	0.37
Co	23	–	28	–	–	–
Co(2 %)Ce	41	11	–	0.0365 ± 0.025	0.044	0.42
Co(12 %)Ce	26	11	17	0.304 ± 0.080	0.15	0.38
Co(2 %)Ce*	24	10	–	0.0573 ± 0.013	0.063	0.21
Co(12 %)Ce*	44	11	25	0.299 ± 0.001	0.073	0.22

Nominal Co/Ce atomic ratios: 0.058 (Co(2 %)Ce) and 0.35 (Co(12 %)Ce).
[a] Crystallite sizes calculated using the Scherrer formula (XRD).

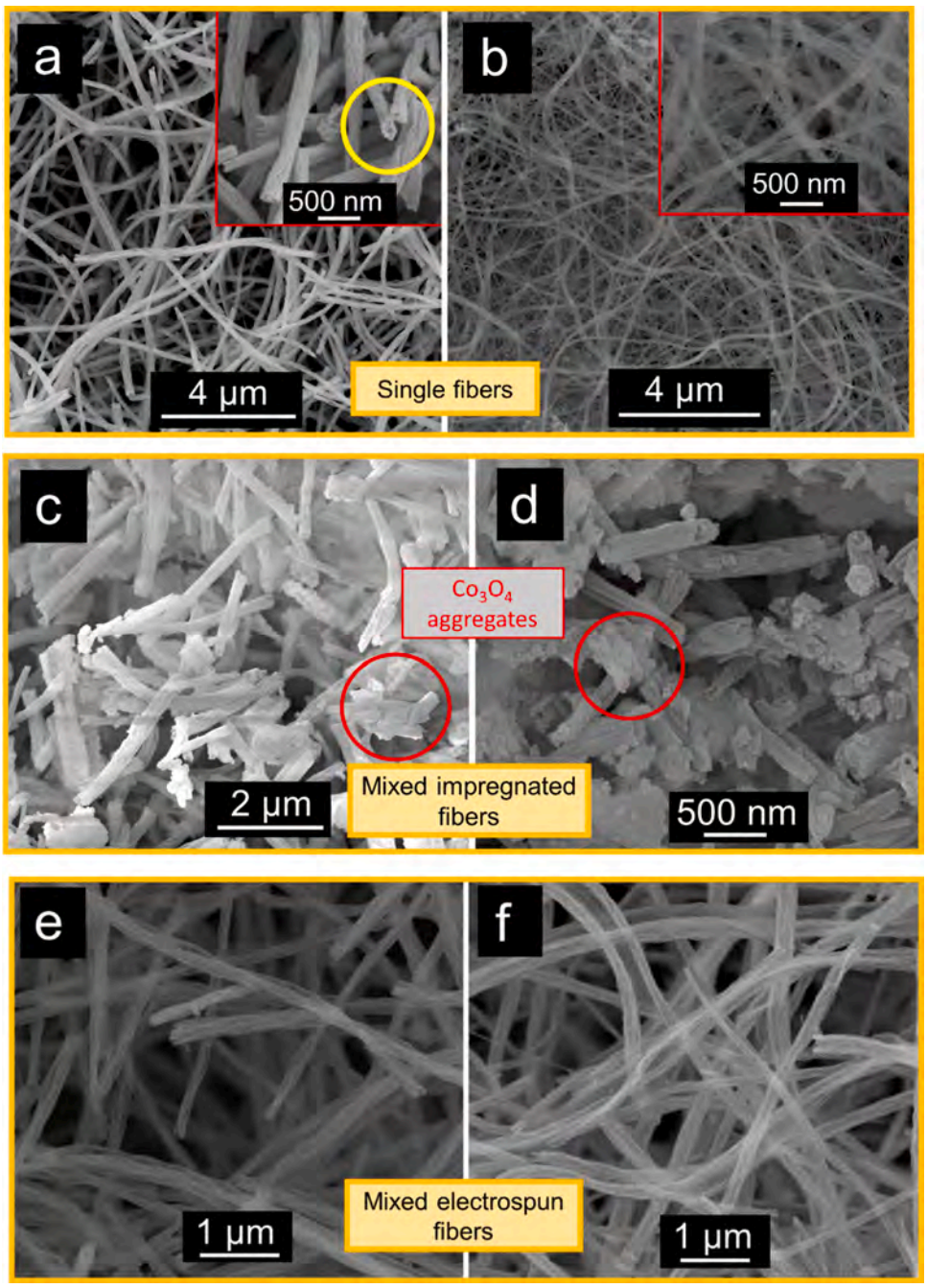

Fig. 2. SEM images of synthesized fibers: Ce (a), Co (b), Co(2 %)Ce (c), Co(12 %)Ce (d), Co(2 %)Ce* (e) and Co(12 %)Ce* (f). (For interpretation of the references to colour in this figure text, the reader is referred to the web version of this article.)

the spectra collected for all the prepared fibers. In the case of those samples containing cobalt, an intense signal between 600 and 700 cm^{-1} appears, which corresponds to the ν_2 vibration mode of Co^{2+}-O at tetrahedral position. A closer inspection (Fig. 3b) shows that this signal is composed of a main peak at 656 cm^{-1} and a shoulder at 674 cm^{-1}, which correspond to the LO (longitudinal optical)/TO (transverse optical) bands of Co_3O_4 [24] and could be detected by the IR reflection mode. This confirms, along with XRD, the formation of the single-phase face-centered spinel structure (Co_3O_4) in cobalt-containing fibers.

Additionally, Fig. 3c shows several bands corresponding to stretching and bending modes of surface carbonates (1536, 1511, 1339, 1054, 966 and 853 cm^{-1}). Thermogravimetric experiments showed an important weight loss between 200 and 300 °C (not shown) due to PVP thermal decomposition, responsible for surface carbonates detected by ATR-FTIR. However, these carbonate species would not affect catalytic activity of electrospun fibers for oxidation reactions since CO_2 is the main product both of CO and soot combustion reactions.

The reducibility of the fibers was studied by CO-TPR (Fig. 4) by monitoring CO_2 formation as the temperature was increased, where the reduction process involves the reaction of CO with surface oxygen species at lower temperatures and with lattice oxygen at higher temperatures.

The profile of bare ceria fibers shows a wide and small peak below 400 °C, while at higher temperatures, the signal is more intense but also broad. The broad signal at lower temperatures is associated with both the reduction of surface OH groups and surface lattice oxygen, whereas the high temperature signal involves the reduction of lattice oxygen [24], as considered by the following reaction:

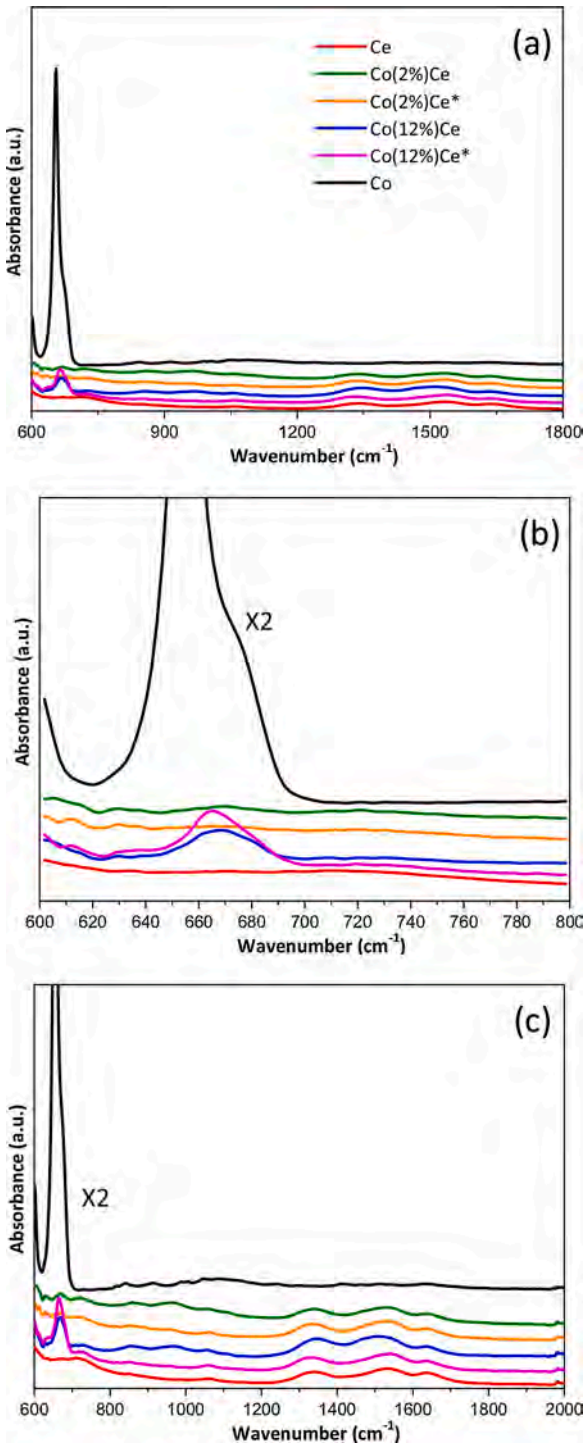

Fig. 3. FTIR spectra of single and mixed fibers (a), different magnifications and scales (b) and (c).

$$2CeO_2 + CO \rightarrow Ce_2O_3 + CO_2$$

On the other hand, for Co_3O_4 nanofibers, the reduction process starts at 250 °C and the CO_2 concentration reaches a maximum at 350 °C. Considering that Co_3O_4 has a spinel structure that contains Co^{3+} in an octahedral coordination and Co^{2+} in a tetrahedral coordination; a reduction profile involving two peaks would be expected, according to the reduction steps Co^{3+} to Co^{2+} (first reduction step) followed by Co^{+2} to Co° (second reduction step) [20], as follows:

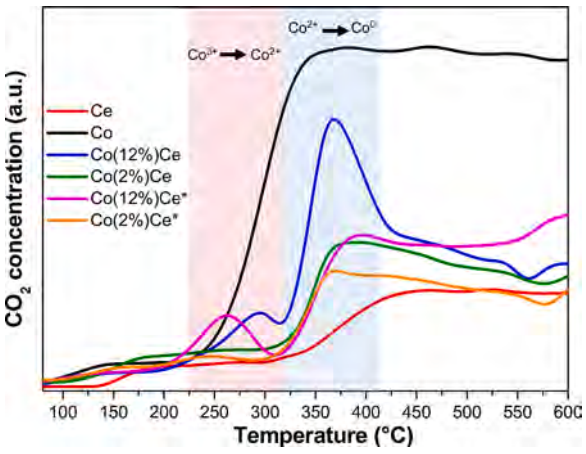

Fig. 4. CO-TPR profiles of the nanofibers.

$$\underbrace{CoO + Co_2O_3}_{Co_3O_4} + CO \rightarrow 3CoO + CO_2 \quad \text{(first reduction step)}$$

$$CoO + CO \rightarrow Co^0 + CO_2 \quad \text{(second reduction step)}$$

However, a plateau in the CO-TPR profile is observed for temperatures higher than 350 °C. When the second reduction step occurs and Co° is formed, the plateau in CO_2 concentration observed may be due to the Boudouard reaction ($2CO \rightarrow C + CO_2$). It is readily known that this reaction in catalyzed by metallic cobalt [25]. Indeed, the formation of carbon during the CO-TPR experiment for Co_3O_4 fibers was verified by a subsequent TPO experiment (Fig. S1).

The CO-TPR profiles for Co(2 %)Ce and Co(2 %)Ce* are similar, showing both samples wide peaks with maxima at 370 °C. As compared with profiles obtained for single ceria fibers, the reduction of both surface and lattice oxygen of ceria takes place along with cobalt reduction. The last is evidenced by the maxima at 370 °C and would be associated with cobalt reduction ($Co^{+2} \rightarrow Co^{\circ}$). However, the profile at lower temperatures compares quite well with that of CeO_2 fibers, indicating low amounts of Co^{3+} in fibers containing 2 wt% Co. This is in agreement with XRD patters, which showed no segregation of Co_3O_4 for these samples, for which cobalt would be mainly incorporated into the CeO_2 lattice and/or forming Co_3O_4 crystallites smaller than 4 nm. Since the radius of the Ce^{4+} cation with octahedral coordination is larger than that of Co^{2+} cation, it is likely that cobalt would be forming a $Co_xCe_{1-x}O_{2-\sigma}$ solid solution [21]. As reported [26,27], cobalt can be introduced into the CeO_2 lattice up to a content of 5 mol% (calculated as 100.Co/(Co + Ce). Therefore, at low Co loadings (2 wt.% =5 mol%), a cobalt–cerium oxide solid solution could has formed, whereas for higher Co loadings (12 wt.%), crystalline Co_3O_4 was observed by XRD. Nevertheless, only the impregnated sample exhibited Co_3O_4 conglomerates deposited on CeO_2 fibers, as observed by SEM images (Fig. 2). That would imply that in the one step synthesized fibers, segregated oxides (CeO_2 and Co_3O_4) would be constituting the fibers and intimately mixed, favoring Co-Ce interaction. This is corroborated with reducibility of cobalt-containing fibers: when increasing the cobalt content from 2 wt.% to 12 wt.% in the impregnated fibers, two peaks in the CO-TPR profile appear, at 292 °C and 365 °C (Co(12 %)Ce), the first corresponding to $Co^{3+} \rightarrow Co^{2+}$ and the second to $Co^{2+} \rightarrow Co^{\circ}$ reduction steps. In the case of the one step synthesized fibers (Co(12 %)Ce*) the low-temperature peak appears shifted to lower temperatures and the high temperature one is less intense than that of the impregnated sample. The higher intensity peak in the second reduction step is related to a higher percentage of segregated Co^{2+} in Co(12 %)Ce fibers, as compared to Co(12 %)Ce* fibers. On the other hand, the shift to lower temperatures corresponding to $Co^{3+} \rightarrow Co^{2+}$ reduction for Co(12 %)Ce* could be related to a higher accessibility of Co^{3+} species in the one step synthesized sample.

The surface composition and chemical states of Ce, Co and Co/Ce

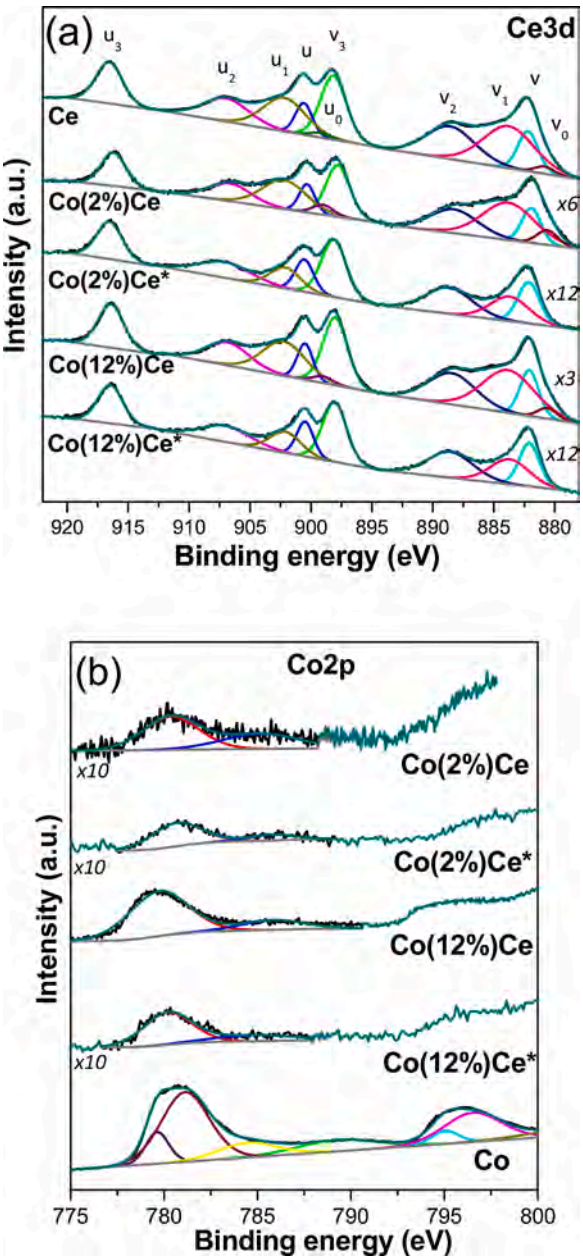

Fig. 5. XPS analysis of Ce3d (a) and Co2p (b) spectra.

catalysts were examined by XPS. The chemical states of Ce were investigated by analyzing the Ce 3d spectra (Fig. 5a). The spectra of Ce 3d could be resolved into ten peaks corresponding to the $3d_{3/2}$ and $3d_{5/2}$ spin-orbit coupling, of which six peaks labeled as v, v_2, v_3, u, u_2, and u_3 are assigned to Ce^{4+}, and for Ce^{3+} state, the peaks are denoted as v_0, v_1, u_0 and u_1 [28]. The spectra of the samples Co(2 %)Ce* and Co(12 %)Ce* were adjusted with eight components, the component u_0 and v_0 (assigned to Ce^{+3}) were not found [29]. The exact position for each assigned peak is listed in Table S1. The proportion of Ce^{3+} to the total Ce (Ce^{3+} and Ce^{4+}) was calculated based on the integrated peak area of Ce^{3+} and Ce^{4+} states and shown Table 1. It is observed that the fibers with cobalt incorporated by synthesis in one step have lower Ce^{+3}/Ce surface ratios (0.21 for Co(2 %)Ce* and 0.22 for Co(12 %)Ce*) as compared to ceria bare nanofibers (0.37). On the contrary, the fibers impregnated with cobalt show a higher Ce^{+3}/Ce surface ratio (0.42 for Co(2 %)Ce and 0.38 for Co(12 %)Ce). The presence of superficial Ce^{3+} may cause more oxygen vacancies and structural defects. The high mobility of oxygen vacancies on the surface of ceria is well-known [30]: Ce^{3+} ions associated with the presence of oxygen vacancies play a critical role in the oxidation mechanism (surface oxygen vacancies) and migration of oxygen toward the surface material (bulk oxygen vacancies) [28].

Fig. 5b illustrates the Co 2p spectra of the samples. The electrospun cobalt nanofibers has two peaks at binding energy values of about 780 eV (Co2p3/2) and 795 eV (Co2p1/2) and the respective shake-up. The satellite peak is ascribed to the cobalt species with valence +2 (Co^{2+}) [31]. The deconvolution of Co2p spectra (Co fibers) revealed the coexistence of both Co^{3+} and Co^{2+} species due to the peaks at 779.6 and 795 eV, 781.1 and 796.5 eV, respectively (Table S2). The binding energy difference between the $Co2p_{1/2}$ and $Co2p_{3/2}$ peaks is about 15.4 eV in agreement with the value reported in the literature for Co_3O_4. In the case of Co-Ce nanofibers it was not possible to assign Co^{2+} and Co^{3+} species, although it was possible to identify the main peak of $Co2p_{3/2}$ and the shake-up.

Table 1 shows the Co/Ce surface atomic ratio results. It is observed that the nanofibers with 2 and 12 % of cobalt (one step synthesis) have a similar surface Co/Ce ratio (0.063 and 0.073, respectively). This could indicate either the migration of the Ce ions to the surface or the migration of Co ions to the bulk during the synthesis process. When incorporating 2 % Co by impregnation (sequential synthesis), a lower surface Co/Ce ratio of the nanofibers is observed (Co/Ce = 0.044) compared to the fibers made by one step synthesis. Nanofibers impregnated with 12 % Co show the highest Co/Ce surface ratio (0.15), but this value is still lower than the nominal bulk content of cobalt, indicating migration of cobalt inside ceria fibers.

XPS spectra of O1s were also measured to examine the different oxygen species present at the surface of the catalysts. As illustrated in

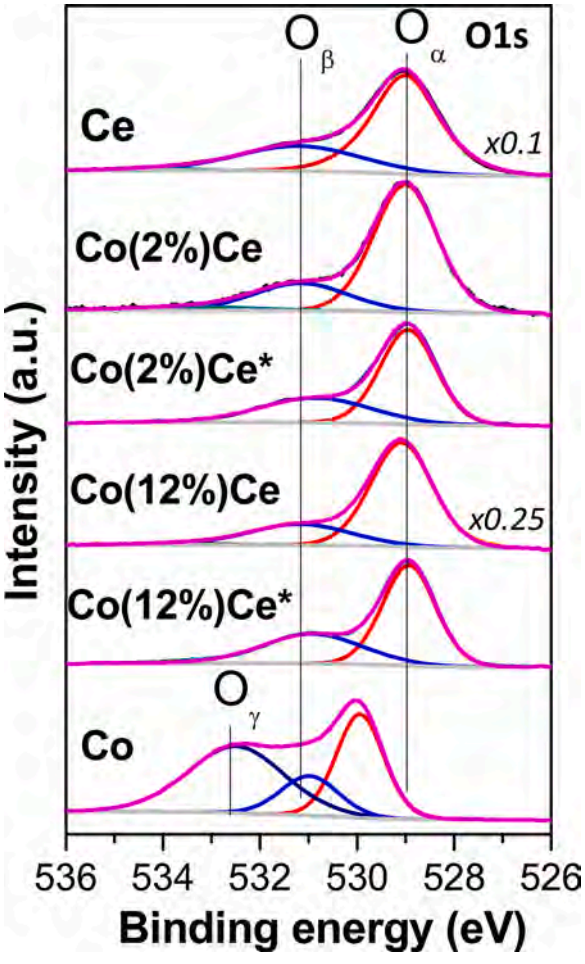

Fig. 6. O1s spectra (XPS). Deconvolution.

Fig. 6, all samples show the main signal close to 529 eV except Co fibers, for which the main signal is shifted about 1 eV towards higher binding energy values. The deconvolution of the O1s spectra shows three or four types of oxygen species. The main peak (O_α) at low binding energy (529−530 eV) is attributed to the lattice surface oxygen in the oxides (O^{2-} species). The peaks located at 531 eV (O_β) are assigned to adsorbed surface oxygen species (OH-, O_2- or O^-), according to the low temperature signals observed from CO-TPR experiments. Superoxide and/or peroxide species are transiently produced by oxygen adsorption on the surface and they contribute in oxidation reactions [32]. In addition, bare Co_3O_4 nanofibers have a peak at 532.5 eV that may be attributed to defect surface oxygen species (O_γ) [33].

The lattice oxygen (O_α) of the oxides with ceria are presented at a binding energy of approximately 529 eV, however for bare cobalt oxide this peak is displaced at 1 eV (~530 eV) [21]. The composition of oxygen on the surface of the oxides plays an important role in the catalytic activity of oxidation reactions. In addition, several authors [34] have shown that the catalytic activity of the solid could be correlated with the presence of a greater number of O_β (and O_γ) species, since these present greater mobility than the lattice oxygen in the oxides. A relationship between O_β (or $O_\beta + O_\gamma$ for Co_3O_4 nanofibers) and O_α species was calculated for all samples and is shown in Table 2. The order of $O_\beta+O_\gamma/O_\alpha$ ratios is as follows: Co > Co-Ce (one step synthesis) > Ce > Co-Ce (sequential synthesis). As reported by Zhang et al. [33], Co_3O_4 catalysts had species of surface oxygen defects as chemisorbed oxygen species, these species act as active oxygen species for oxidation reactions. The cobalt fibers studied in this work have a large proportion of O_γ, while the Ce and Co-Ce fibers do not have O_γ species.

3.2. Soot oxidation

The activity of catalytic fibers for diesel soot combustion (TPO experiments) is shown in Fig. 7a, where soot conversion and CO_2 production curves vs. temperature are depicted. In all profiles, a wide peak of CO_2 formation can be observed at low temperatures, between 200−250 °C. This peak is related to the oxidation of n-hexane used to prepare the suspension used to incorporate soot to catalytic fibers. The soot oxidation occurs between 300−450 °C for all nanofibers, and it should be noted that these burning temperatures are very good values, since the temperatures of diesel exhaust are in this range [35].

Considering the individual behavior of nanofibers in the combustion of soot, it can be seen that ceria and cobalt fibers have maxima combustion temperatures at around 380 °C. Although T_M values are similar, the profiles are different, since ceria shows a wider burning temperature range and cobalt fibers show a narrower one. Co-Ce nanofibers show a higher catalytic activity with respect to that of bare ceria or cobalt fibers, and this is in agreement with many works where the mixed oxide fibers show a synergistic effect of cobalt and cerium [26,36]. Mixed fibers show T_M values around 360 °C, despite the preparation method or the cobalt content.

Many effective catalytic systems have been proposed for soot combustion and other oxidation reactions [8,37]. Due to their unique physicochemical properties, especially the high redox properties and lability of the oxygen lattice, ceria and ceria based materials show high catalytic activity in total oxidation reactions, and oxidation of soot to carbon dioxide is no an exception. Ceria also has a high oxygen storage

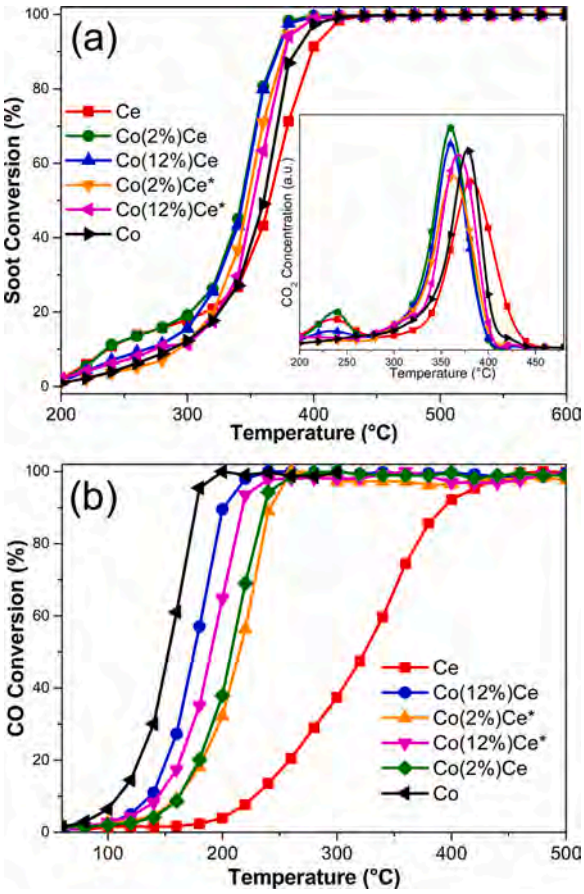

Fig. 7. Catalytic activity of the nanofibers in the oxidation of diesel soot (a) and in the oxidation of carbon monoxide (b).

capacity (OSC), which allows the oxide to be used not only as a support or modifying additive, but also as a catalyst for the oxidation of soot.

According to Machida et al. [38], the redox properties of ceria are an important factor, but not the main one, for the catalytic oxidation of soot. Morphology is known to play an important role in solid-solid reactions, where the number of contact points is a crucial criterion for activity.

Therefore, the size, diameter and weft of nanofibers made by means of electrospinning synthesis produces a network of fibers which is a key factor in generating several contact points between soot particles and the catalytic nanofibers, enhancing reactivity in this solid-solid reaction. In addition, an improvement of 20 °C in the oxidation of soot is achieved when using mixed oxides of cobalt-ceria, and this improvement in performance could be directly related to a synergy between the oxides, improving the redox properties of the fibers. The results of the characterization of the catalysts suggest the formation of a solid solution when incorporating low cobalt contents (2 wt.% Co) in Co-Ce fibers. The interaction between cobalt and ceria is observed both for the samples prepared by one-step synthesis and sequential synthesis. The Co_3O_4-CeO_2 interaction produces a synergistic effect, mainly due to the

Table 2
Binding energy values of O1s species obtained from curve fitting (Fig. 6) and O_β /O_α atomic ratio.

Sample	O_α BE(eV) (at.%)	O_β BE (eV) (at.%)	O_γ BE (eV) (at.%)	$(O_\beta+O_\gamma)$ /O_α
Ce	529.1 (68.4)	531.3 (30.4)	–	0.44
Co	529.9 (36.1)	531.0 (16.8)	532.5 (47.1)	1.77
Co(2 %)Ce	529 (72.7)	531.1 (23.1)	–	0.32
Co(12 %)Ce	529.1(74.1)	531.2 (26.6)	–	0.36
Co(2 %)Ce*	529 (65.9)	530.8 (34)	–	0.51
Co(12 %)Ce*	529.0 (64.3)	530.9 (35.7)	–	0.55

combination of Ce^{3+}/Ce^{4+} and Co^{2+}/Co^{3+} redox couples at the surface of the fibers where the soot oxidation takes place. Besides, a cooperative effect between cobalt and cerium oxides should also be considered.

As previously stated, the morphology, size and diameter of ceramic fibers also play a key role in solid-solid-gas reactions. Comparing the activities of Co-Ce catalysts supported on other structured fibers (ceramic papers and wire mesh monoliths), electrospun fibers showed a better performance. While for Co-Ce electrospun fibers T_M is 360 °C, for sprayed ceramic papers is 453 °C, 480 °C for impregnated ceramic papers [11] and 409 °C for Co-Ce supported on wire mesh monoliths which included a bed of Pt,Ce upstream to enhance NO_2 formation [16].

However, although Co-Ce fibers present higher activity than Co and Ce ones, the maximum reaction rate occurs at T_M values that are in a relatively narrow temperature range (350−390 °C). This could be related to the presence of nitric oxide in the feed, in a concentration close to that observed in practical conditions. It is readily known that Co and Ce oxides are capable of easily convert NO into NO_2, which in turn is a strong oxidant that highly contributes to soot combustion. Thus, the differences of T_M for the different fibers are not so important. These results are in line with those reported by Megarajan et al. [39] and Xu et al. [40], who reported the high activity of ceria supported cobalt catalysts for NO oxidation and its impact on soot oxidation. Moreover in reference 36, it is shown that the activity for NO oxidation of Co-Ce mixed oxides is higher than that of the corresponding single oxides. The same trend is observed for the NO_x-assisted soot oxidation by Medina et al. [41]. In our case, the trend found for soot oxidation activity is similar, being the differences in T_M values rather small. As previously discussed, this could be ascribed to the fiber structure morphology.

The promotion mechanism in presence of NO can be interpreted in terms of the following steps reported in the literature [42–44]:

$$NO + 1/2O_2 \rightarrow NO_2 \quad \text{catalyzed by Ce, Co}$$

$$C + NO_2 \rightarrow —C(O) + NO$$

$$—C(O) + NO_2 \rightarrow CO_2 + NO$$

$$NO_2 + (O) \rightarrow NO_3$$

$$—NO_3 \rightarrow —O_2^- + NO$$

$$C + —O_2^- \rightarrow CO_2$$

The differences in surface area and crystallite sizes appear also not influence the catalytic behavior, probable because the soot oxidation reaction takes place at the external surface of the fibers, the diameters of the fibers being similar (between 100−200 nm). Additionally, the reducibility of our samples under CO atmosphere would not play a relevant role for soot combustion, being the key factors, the activity for NO oxidation and the fiber morphology.

3.3. CO oxidation

The CO oxidation reaction was studied using nanofibers as catalysts, the conversion versus temperature profiles obtained are shown in Fig. 7b. When comparing the catalytic behavior of the different fibers synthesized, the CO oxidation conversion trend is quite different as compared to that of diesel soot combustion.

Ceria bare fibers showed the lowest catalytic activity (T_{50} = 325 °C) and the cobalt fibers the highest catalytic activity (T_{50} = 150 °C), the difference of T_{50} being 175 °C in these fibers. Co-Ce nanofibers show intermediate catalytic activity compared to bare fibers, being higher when the fibers contain a higher percentage of cobalt. In fact, fibers with 12 wt.% Co are more active compared to nanofibers with 2 wt.% Co, furthermore, the fibers with cobalt incorporated by impregnation show greater performance. This observation in activity is in agreement with the CO-TPR results discussed above.

The Mars-van Krevelen mechanism has been widely adopted for explaining CO oxidation over CeO_2 supported transition metal oxide catalysts which involves the reaction between chemisorbed CO with surface lattice oxygen species of Co-Ce, thus forming oxygen vacancies. Then, the replenishment of the as-formed oxygen vacancies by gas-phase oxygen or a “lattice-oxygen” migration process will occur during the reaction [45].

Observing the performance of fibrous catalysts for CO oxidation, cobalt spinel fibers turn out to be more active. CO oxidation is a structure sensitive reaction, that is, exposure of different crystal planes of oxides shows different activity for CO oxidation [46]. Considering the sizes and diameter of the fibers, the bare cobalt fibers have the smallest diameter. In contrast, the improvement in the activity related to the bulk and surface structure of the fibers should also be taken into account. From XPS results, the naked cobalt fibers show superficial oxygen species (O_γ) that the other fibers do not have. These species of oxygen can be key in the best activity and reducibility of Co_3O_4 fibers. Catalytic results show that the performance of fibers for both reactions is quite different, the cobalt fibers being the most active for CO oxidation and the Co-Ce fibers being the most active for soot oxidation. These results are probably related to the different nature of these reactions, where the contact of the catalyst with the reagents seems to be an important point for the oxidation of soot. As said before, the presence of NO in the feed also contributes to the catalytic behavior of the fibers during soot oxidation reaction.

Fig. 8 shows the calculated apparent activation energies for each synthesized fiber for CO oxidation. The energies are in a range of 12–15 KJ/mol, being in agreement with is reported by these catalytic systems, therefore these differences do not explain the differences in the catalytic performance for CO oxidation. CO TPR experiments, show that the reduction capacity of the fibers follows the order Co > Co(12 %)Ce > Co (12 %)Ce* > Co(2 %)Ce ≈ Co(2 %)Ce* > Ce, which matches exactly with the trend in catalytic activity for CO oxidation that is shown in Fig. 9, which is not the case for soot oxidation. This implies that Co should be included in the active sites for CO oxidation, it can be suggested that Co_3O_4 bare or CeO_2/Co_3O_4 interface sites are active for CO oxidation, whereas bare CeO_2 has low activity in our experimental conditions. The differences could be related to the cobalt bulk content as well as the role played by the different oxygen species present in the catalyst. For the soot oxidation, it has been reported that labile chemisorbed oxygen, could be the oxygen species that determine the catalytic behavior of Co-Ce catalysts when they are in the form of biomorphic structures. This surface species could be the responsible for the oxidation of soot and the formation of NO_2 that in turn also contributes to soot oxidation [47]. For CO oxidation, instead, the agreement in temperature

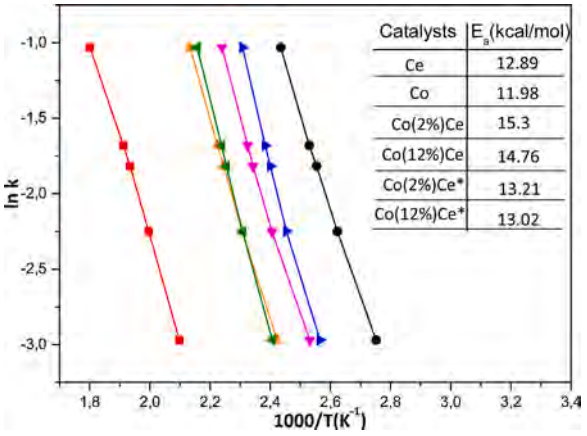

Fig. 8. Pseudo-first order CO oxidation: Arrhenius plots. Catalysts: (red) Ce, (green) Co(2 %)Ce, (orange) Co(2 %)Ce*, (blue) Co(12 %)Ce, (magenta) Co(12 %)Ce* and (black) Co fibers. (For interpretation of the references to colour in this figure legend, the reader is referred to the web version of this article.)

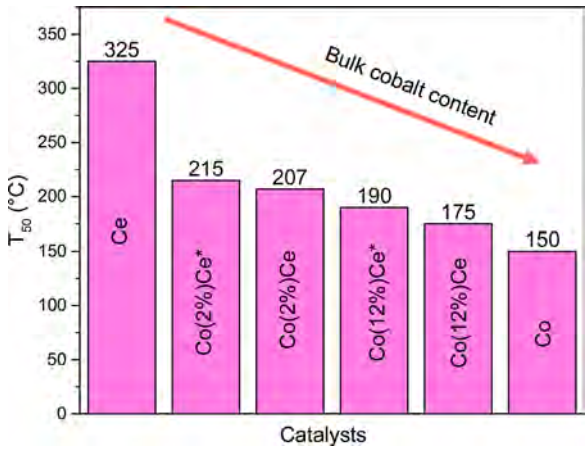

Fig. 9. Plots that relates the T_{50} in the CO oxidation versus different catalytic fibers.

trends observed for CO oxidation and CO-TPR strongly suggests the key role of lattice species, specially associated with Co^{2+} species. Fig. 9 clearly shows the correlation of these species and T_{50}.

4. Conclusions

The electrospinning method allowed us to obtain single and mixed Co,Ce fibers with a nanometric diameter forming a net of interconnected fibers. In the solid-solid-gas reaction studied (soot oxidation), the nanometric diameter is found to be a key factor in improving performance, allowing higher contact points between soot and catalyst, as well as the synergistic effect in the mixed Co-Ce oxides. As a matter of fact, T_M for electrospun samples resulted lower as compared with Co-Ce supported on micrometric fibers. On the other hand, in the gas-solid reaction studied (CO oxidation), the reducibility of the studied oxides is a key factor, being the diameter and size of these fibers less important. The improvement in catalytic performance in CO oxidation is closely related to the increase in cobalt content. Cobalt bare fibers are more active than mixed fibers, indicating that the main active sites in Co-Ce fibers are Co species.

CRediT authorship contribution statement

M. Ángeles Stegmayer: Conceptualization, Data curation, Formal analysis, Investigation, Methodology, Software, Validation, Visualization, Writing - original draft. **Silvia Irusta:** Formal analysis, Investigation, Methodology, Project administration, Resources, Writing - review & editing. **Eduardo E. Miró:** Conceptualization, Data curation, Formal analysis, Funding acquisition, Investigation, Methodology, Project administration, Resources, Supervision, Validation, Visualization, Writing - review & editing. **Viviana G. Milt:** Conceptualization, Data curation, Formal analysis, Funding acquisition, Investigation, Methodology, Project administration, Resources, Supervision, Validation, Visualization, Writing - review & editing.

Declaration of Competing Interest

The authors report no declarations of interest.

Acknowledgments

The authors wish to acknowledge the financial support received from ANPCyT (Grant PME 87-PAE 36985 to purchase the RAMAN Instrument and PICT 2016–2710), CONICET and UNL.

Appendix A. Supplementary data

Supplementary material related to this article can be found, in the online version, at doi:https://doi.org/10.1016/j.cattod.2020.12.018.

References

[1] E. Reichelt, M.P. Heddrich, M. Jahn, A. Michaelis, Fiber based structured materials for catalytic applications, Appl. Catal. A Gen. 476 (2014) 78–90, https://doi.org/10.1016/j.apcata.2014.02.021.
[2] N.A. Sacco, E.D. Banús, J.P. Bortolozzi, V.G. Milt, E.E. Miró, Ultrasound-assisted deposition of Co-CeO_2 onto ceramic microfibers to conform catalytic papers: their application in engine exhaust treatment, ACS Omega 3 (2018) 18334–18342, https://doi.org/10.1021/acsomega.8b02949.
[3] P.A. Kumar, M.D. Tanwar, S. Bensaid, N. Russo, D. Fino, Soot combustion improvement in diesel particulate filters catalyzed with ceria nanofibers, Chem. Eng. J. 207–208 (2012) 258–266, https://doi.org/10.1016/j.cej.2012.06.096.
[4] I. Moreno, N. Navascues, S. Irusta, J. Santamaria, Electrospun Au/CeO_2 nanofibers: a highly accessible low-pressure drop catalyst for preferential CO oxidation, J. Catal. 329 (2015) 479–489, https://doi.org/10.1016/j.jcat.2015.06.011.
[5] Y. Dai, J. Tian, W. Fu, Shape manipulation of porous CeO_2 nanofibers: facile fabrication, growth mechanism and catalytic elimination of soot particulates, J. Mater. Sci. 54 (2019) 10141–10152, https://doi.org/10.1007/s10853-019-03648-9.
[6] J.M. López, A.L. Gilbank, T. García, B. Solsona, S. Agouram, L. Torrente-Murciano, The prevalence of surface oxygen vacancies over the mobility of bulk oxygen in nanostructured ceria for the total toluene oxidation, Appl. Catal. B Environ. 174–175 (2015) 403–412, https://doi.org/10.1016/j.apcatb.2015.03.017.
[7] M.Á. Stegmayer, V.G. Milt, N. Navascues, E. Gamez, S. Irusta, E.E. Miró, Cobalt deposited on micro and nanometric structures of ceria and zirconia applied in diesel soot combustion, Mol. Catal. 481 (2020), 100636, https://doi.org/10.1016/j.mcat.2018.07.011.
[8] A.M. Hernández-Giménez, D.L. Castelló, A. Bueno-López, Diesel soot combustion catalysts: review of active phases, Chem. Pap. 68 (2014) 1154–1168, https://doi.org/10.2478/s11696-013-0469-7.
[9] M. Lykaki, E. Pachatouridou, S.A.C. Carabineiro, E. Iliopoulou, C. Andriopoulou, N. Kallithrakas-Kontos, S. Boghosian, M. Konsolakis, Ceria nanoparticles shape effects on the structural defects and surface chemistry: Implications in CO oxidation by Cu/CeO_2 catalysts, Appl. Catal. B Environ. 230 (2018) 18–28, https://doi.org/10.1016/j.apcatb.2018.02.035.
[10] T. Montini, M. Melchionna, M. Monai, P. Fornasiero, Fundamentals and catalytic applications of CeO_2-based materials, Chem. Rev. 116 (2016) 5987–6041, https://doi.org/10.1021/acs.chemrev.5b00603.
[11] S.A. Leonardi, F.E. Tuler, E.M. Gaigneaux, D.P. Debecker, E.E. Miró, V.G. Milt, Novel ceramic paper structures for diesel exhaust purification, Environ. Sci. Pollut. Res. 25 (2018) 35276–35286, https://doi.org/10.1007/s11356-018-3439-3.
[12] A. Chiodoni, D. Fino, M. Piumetti, F. Giorgis, N. Russo, S. Bensaid, C. Novara, Catalytic oxidation of CO and soot over Ce-Zr-Pr mixed oxides synthesized in a multi-inlet Vortex reactor: effect of structural defects on the catalytic activity, Nanosc. Res. Lett. 11 (2016) 1–14, https://doi.org/10.1186/s11671-016-1713-1.
[13] C. Lee, Y. Jeon, T. Kim, A. Tou, J. Il Park, H. Einaga, Y.G. Shul, Ag-loaded cerium-zirconium solid solution oxide nano-fibrous webs and their catalytic activity for soot and CO oxidation, Fuel 212 (2018) 395–404, https://doi.org/10.1016/j.fuel.2017.10.007.
[14] S. Liu, X. Wu, D. Weng, R. Ran, Ceria-based catalysts for soot oxidation: a review, J. Rare Earths. 33 (2015) 567–590, https://doi.org/10.1016/S1002-0721(14)60457-9.
[15] M. Dosa, M. Piumetti, S. Bensaid, T. Andana, C. Novara, F. Giorgis, D. Fino, N. Russo, Novel Mn–Cu-containing CeO_2 nanopolyhedra for the oxidation of CO and diesel soot: effect of dopants on the nanostructure and catalytic activity, Catal. Letters 148 (2018) 298–311, https://doi.org/10.1007/s10562-017-2226-y.
[16] M.L. Godoy, E.D. Banús, E.E. Miró, V.G. Milt, Single and double bed stacked wire mesh cartridges for the catalytic treatment of diesel exhausts, J. Environ. Chem. Eng. 7 (2019), 103290, https://doi.org/10.1016/j.jece.2019.103290.
[17] E.D. Banús, V.G. Milt, E.E. Miró, M.A. Ulla, Co,Ba,K/ZrO_2 coated onto metallic foam (AISI 314) as a structured catalyst for soot combustion: coating preparation and characterization, Appl. Catal. A Gen. 379 (2010) 95–104, https://doi.org/10.1016/j.apcata.2010.03.009.
[18] B. Lin, Y. Liu, L. Heng, J. Ni, J. Lin, L. Jiang, Effect of ceria morphology on the catalytic activity of Co/CeO_2 catalyst for ammonia synthesis, Catal. Commun. J. 101 (2017) 15–19, https://doi.org/10.1016/j.catcom.2017.07.015.
[19] X. Lin, S. Li, H. He, Z. Wu, J. Wu, L. Chen, D. Ye, M. Fu, Evolution of oxygen vacancies in MnO_x-CeO_2 mixed oxides for soot oxidation, Appl. Catal. B Environ. 223 (2018) 91–102, https://doi.org/10.1016/j.apcatb.2017.06.071.
[20] C. Wang, C. Zhang, W. Hua, Y. Guo, G. Lu, S. Gil, A. Giroir-Fendler, Catalytic oxidation of vinyl chloride emissions over Co-Ce composite oxide catalysts, Chem. Eng. J. 315 (2017) 392–402, https://doi.org/10.1016/j.cej.2017.01.007.
[21] X. Li, X. Li, X. Zeng, T. Zhu, Correlation between the physicochemical properties and catalytic performances of micro/mesoporous $CoCeO_x$ mixed oxides for propane combustion, Appl. Catal. A Gen. 572 (2019) 61–70, https://doi.org/10.1016/j.apcata.2018.12.026.
[22] C.L. Bolívar-Díaz, J.C. Conesa, V. Cortés Corberán, M. Monte, A. Martínez-Arias, Nanostructured catalysts based on combinations of cobalt and cerium oxides for

CO oxidation and effect of the presence of water, J. Nanosci. Nanotechnol. 17 (2017) 3816–3823, https://doi.org/10.1166/jnn.2017.14002.
[23] A. Haider, S. Haider, I.K. Kang, A comprehensive review summarizing the effect of electrospinning parameters and potential applications of nanofibers in biomedical and biotechnology, Arab. J. Chem. 11 (2018) 1165–1188, https://doi.org/10.1016/j.arabjc.2015.11.015.
[24] Y. Li, W. Qiu, F. Qin, H. Fang, V.G. Hadjiev, D. Litvinov, J. Bao, Identification of cobalt oxides with Raman scattering and fourier transform infrared spectroscopy, J. Phys. Chem. C 120 (2016) 4511–4516, https://doi.org/10.1021/acs.jpcc.5b11185.
[25] J. Horlyck, C. Lawrey, E.C. Lovell, R. Amal, J. Scott, Elucidating the impact of Ni and Co loading on the selectivity of bimetallic NiCo catalysts for dry reforming of methane, Chem. Eng. J. 352 (2018) 572–580, https://doi.org/10.1016/j.cej.2018.07.009.
[26] J. Liu, Z. Zhao, J. Wang, C. Xu, A. Duan, G. Jiang, Q. Yang, The highly active catalysts of nanometric CeO_2-supported cobalt oxides for soot combustion, Appl. Catal. B Environ. 84 (2008) 185–195, https://doi.org/10.1016/j.apcatb.2008.03.017.
[27] J. Wang, M. Shen, J. Wang, J. Gao, J. Ma, S. Liu, CeO_2-CoO_x mixed oxides: structural characteristics and dynamic storage/release capacity, Catal. Today 175 (2011) 65–71, https://doi.org/10.1016/j.cattod.2011.03.004.
[28] H. Li, F. Meng, J. Gong, Z. Fan, R. Qin, Structural, morphological and optical properties of shuttle-like CeO_2 synthesized by a facile hydrothermal method, J. Alloys Compd. 722 (2017) 489–498, https://doi.org/10.1016/j.jallcom.2017.06.156.
[29] Y. Sun, X. Li, Template-free hydrothermal synthesis and optical properties of ceria hollow nanospheres with rough surface, J. Mater. Sci. Mater. Electron. 28 (2017) 14185–14189, https://doi.org/10.1007/s10854-017-7274-y.
[30] A. Trovarelli, Catalysis by Ceria and related materials, Catal. Sci. Seri.-Vol. 2 (2002).
[31] S. Zhang, S. Liu, X. Zhu, Y. Yang, W. Hu, H. Zhao, R. Qu, C. Zheng, X. Gao, Low temperature catalytic oxidation of propane over cobalt-cerium spinel oxides catalysts, Appl. Surf. Sci. 479 (2019) 1132–1140, https://doi.org/10.1016/j.apsusc.2019.02.118.
[32] L.F. Liotta, M. Ousmane, G. Di Carlo, G. Pantaleo, G. Deganello, G. Marcì, L. Retailleau, A. Giroir-Fendler, Total oxidation of propene at low temperature over Co_3O_4-CeO_2 mixed oxides: role of surface oxygen vacancies and bulk oxygen mobility in the catalytic activity, Appl. Catal. A Gen. 347 (2008) 81–88, https://doi.org/10.1016/j.apcata.2008.05.038.
[33] X. Zhang, H. Zhang, H. Zhu, C. Li, N. Zhang, J. Bao, G. He, Co_3O_4 nanorods with a great amount of oxygen vacancies for highly efficient Hg^0 oxidation from coal combustion flue gas, Energy Fuels 33 (2019) 6552–6561, https://doi.org/10.1021/acs.energyfuels.9b00765.
[34] W. Tang, J. Weng, X. Lu, L. Wen, A. Suburamanian, C.Y. Nam, P.X. Gao, Alkali-metal poisoning effect of total CO and propane oxidation over Co_3O_4 nanocatalysts, Appl. Catal. B Environ. 256 (2019), 117859, https://doi.org/10.1016/j.apcatb.2019.117859.
[35] G.C. Dhal, S. Dey, D. Mohan, R. Prasad, Simultaneous abatement of diesel soot and NO_X emissions by effective catalysts at low temperature: an overview, Catal. Rev. - Sci. Eng. 60 (2018) 437–496, https://doi.org/10.1080/01614940.2018.1457831.
[36] P.A. Kumar, M.D. Tanwar, N. Russo, R. Pirone, D. Fino, Synthesis and catalytic properties of CeO_2 and Co/CeO_2 nanofibres for diesel soot combustion, Catal. Today 184 (2012) 279–287, https://doi.org/10.1016/j.cattod.2011.12.025.
[37] B.R. Stanmore, J.F. Brilhac, P. Gilot, The oxidation of soot: a review of experiments, mechanisms and models, Carbon 39 (2001) 2247–2268, https://doi.org/10.1016/S0008-6223(01)00109-9.
[38] M. Machida, Y. Murata, K. Kishikawa, D. Zhang, K. Ikeue, On the reasons for high activity of CeO_2 catalyst for soot oxidation, Chem. Mater. 20 (2008) 4489–4494, https://doi.org/10.1021/cm800832w.
[39] S. Kumar Megarajan, S. Rayalu, Y. Teraoka, N. Labhsetwar, High NO oxidation catalytic activity on non-noble metal based cobalt-ceria catalyst for diesel soot oxidation, J. Mol. Catal. A Chem. 385 (2014) 112–118, https://doi.org/10.1016/j.molcata.2014.01.026.
[40] J. Xu, G. Lu, Y. Guo, Y. Guo, X. Gong, A highly effective catalyst of Co-CeO_2 for the oxidation of diesel soot: the excellent NO oxidation activity and NO_x storage capacity, Appl. Catal. A Gen. 535 (2017) 1–8, https://doi.org/10.1016/j.apcata.2017.02.005.
[41] J.C. Medina, S.E. Rodil, R. Zanella, Synthesis of a CeO_2/Co_3O_4 catalyst with a remarkable performance for the soot oxidation reaction, Catal. Sci. Technol. 10 (2020) 853–863, https://doi.org/10.1039/c9cy01821b.
[42] Y. Liang, X. Ding, J. Dai, M. Zhao, L. Zhong, J. Wang, Y. Chen, Active oxygen-promoted NO catalytic on monolithic Pt-based diesel oxidation catalyst modified with Ce, Catal. Today (2019) 64–72, https://doi.org/10.1016/j.cattod.2018.06.008.
[43] W.F. Shangguan, Y. Teraoka, S. Kagawa, Kinetics of soot-O_2, soot-NO and soot-O_2-NO reactions over spinel-type $CuFe_2O_4$ catalyst, Appl. Catal. B Environ. 12 (1997) 237–247, https://doi.org/10.1016/S0926-3373(96)00076-8.
[44] H. Zhang, S. Li, Q. Lin, X. Feng, Y. Chen, J. Wang, Study on hydrothermal deactivation of Pt/MnO_x-CeO_2 for NO_x-assisted soot oxidation: redox property, surface nitrates, and oxygen vacancies, Environ. Sci. Pollut. Res. 25 (2018) 16061–16070, https://doi.org/10.1007/s11356-018-1582-5.
[45] Z. Liu, J. Li, R. Wang, CeO_2 nanorods supported M–Co bimetallic oxides (M = Fe, Ni, Cu) for catalytic CO and C_3H_8 oxidation, J. Colloid Interface Sci. 560 (2020) 91–102, https://doi.org/10.1016/j.jcis.2019.10.046.
[46] S. Dey, G.C. Dhal, D. Mohan, R. Prasad, Synthesis of highly active Cobalt catalysts for low temperature CO oxidation, Chem. Data Collect. 24 (2019), 100283, https://doi.org/10.1016/j.cdc.2019.100283.
[47] M.Á. Stegmayer, V.G. Milt, E.E. Miró, Biomorphic synthesis of cobalt oxide and ceria microfibers. Their application in diesel soot oxidation, Catal. Commun. 139 (2020), 105984, https://doi.org/10.1016/j.catcom.2020.105984.